scientific reports

Check for updates

OPEN

Influence of portal excavation of shallow-buried bias tunnel on stability of soil–rock bedding slope: a case study of Moziping tunnel

Tao Li[1,2,3], Yue Li[2✉], Jiajun Shu[2], Shiming Hu[2] & Bo Liu[1,2,3]

The excavation of tunnel portals in shallowly buried bias tunnels in mountainous areas is highly prone to causing instability of the soil–rock bedding slopes at portals, which threatens project safety. This paper uses the Moziping tunnel outlet section as the engineering background. A research approach that combines theoretical analysis, numerical simulation, and field monitoring is adopted to systematically investigate the impact mechanism of tunnel excavation on the stability of soil–rock bedding slopes. A mechanical model of a tunnel–soil–rock bedding slope is established on the basis of the transfer coefficient method, and a slope stability evaluation method suitable for composite strata is proposed. Additionally, the slope deformation pattern and failure modes under tunnel portal excavation are revealed. The research results indicate that the stability coefficients of the slope after tunnel excavation obtained from theoretical calculations and numerical simulations are 1.18 and 1.13, respectively, with a difference of only 4%, thereby validating the reliability of the proposed theoretical method. As the tunnel excavation distance increases, the slope deformation exhibits three characteristic stages: the rapid deformation stage (excavation distance ≤ 0.22D), which contributes 78.1% to 81.1% of the total deformation; the slow deformation stage (0.22D–2.63D), accompanied by partial rebound; and the stable stage (> 2.63D), where the deformation tends to stabilize. The interlayer sliding effect at the soil–rock interface results in significant horizontal displacement, which promotes the formation of a potential slip surface at the slope's forefront. This is manifested as the convergence value of the upper-step surrounding rock being significantly greater than that of the lower step. The plastic strain concentration at the toe of the shallowly buried side slope is a key trigger for slope instability, which is consistent with the development characteristics of shear cracks observed in the field. The research findings provide a theoretical basis for evaluating the stability of soil–rock layered slopes and safe tunnel construction.

In recent years, China has gradually increased the construction of highway tunnels in mountainous areas to promote economic development[1,2]. However, owing to the complex and changeable geological conditions in the southwest mountainous area, the tunnel excavation process often causes slope instability problems, especially bedding slopes[3,4]. Bedding slopes are often the most susceptible to sliding hazards because of their special structural characteristics[5–7]. Bedded landslides are widely found in East Sichuan and the Three Gorges Reservoir area[8–11], and there are more than 500 landslides in the Wanzhou area alone, of which bedded landslides account for more than 90% of the total landslides[12,13]. Tunnelling within bedding slopes disrupts the original balance of the mountain, and weathered laminations or weak interfaces reduce the shear strength of the rock mass, leading to geologic hazards such as laminar sliding or collapse[14–16]. Therefore, the slope stability of soil-rock bedding under the disturbance of tunnel portal excavation needs urgent attention.

Many scholars have researched the impact of tunnel excavation on slope stability. Kaya et al.[17] analyzed the stability of tunnel slopes via the limit equilibrium method and explored the effects of different treatment

[1]Inner Mongolia Research Institute, China University of Mining and Technology (Beijing), Ordos 017004, China. [2]School of Mechanics and Civil Engineering, China University of Mining and Technology (Beijing), Beijing 100083, China. [3]State Key Laboratory for Tunnel Engineering, China University of Mining and Technology (Beijing), Beijing 100083, China. ✉email: X1360141107@163.com

measures on their stability. Zhang et al.[18] studied the mechanical properties of loose rock masses at tunnel entrances on the basis of linear slip theory. They determined the scope of tunnel disturbance and the minimum safe distance between the arch and the slip zone. The unloading effect caused by tunnel excavation leads to subsidence of the soil column above the tunnel and transmits forces to the surrounding rock. When the forces exceed the strength of the rock and soil, cracks are created in the soil column and extend to the surface. In addition, tunnel excavation will cause cracks in the slope sliding body, resulting in the sliding body blocking and causing stress redistribution in the surrounding rock, thus affecting the sliding thrust[19–21]. Wang et al.[22] proposed a prediction method for the landslide range on the basis of the failure mode of the rock surrounding the slope after tunnel excavation disturbance. Cai et al.[23] proposed an analytical approximate solution for stresses and displacements around multiple shallow circular tunnels in sloping terrain considering inter-tunnel interactions. Zhang et al.[24] studied the interaction between tunnel excavation and rock slope stability via model tests and numerical simulations. Song et al.[25–28] used the finite element method to study the important influence of tunnel excavation on rock slope stability. Chen et al.[29] systematically investigated the stepped failure mechanism of water-bearing rock slopes using particle flow numerical simulation and conducted quantitative stability assessment. Tian et al.[30] studied the deformation and mechanical properties of the tunnel-slope system containing existing anti-slip piles under pile-wall replacement structure. Tian et al.[31] studied the deformation characteristics and failure mode of rock slopes with clay interlayers under tunnel excavation conditions through field monitoring and numerical simulation. Qin et al.[32] investigated the impact of tunnel construction on the stability of loess slopes, focusing on disturbance-induced failure triggers, unique loess behavior mechanisms, and instability processes. Ding et al.[33] analyzed the deformation mechanism and stability of geotechnical slopes under excavation disturbance and fissure seepage based on long-term monitoring data and FLAC 3D numerical simulation. Tian et al.[34] analyzed the disaster mechanism of the tunnel-slope system and proposed reinforcement measures, taking the Hanshankou Tunnel as an engineering example. Song et al.[35,36] emphasized the importance of in situ monitoring in slope stability studies. The numerical method may lead to uncertainty in the calculation results when the geological parameters and boundary conditions are simplified, which needs to be further verified via field monitoring.

Currently, research on the impact of tunnel excavation on slope stability and deformation mechanisms has focused primarily on rocky slopes with weak structural planes or homogeneous slopes. There is a lack of universal theoretical models applicable to soil–rock layered composite slopes. In addition, the deformation evolution mechanism of soil–rock layered slopes under the disturbance of shallowly buried tunnel portal excavation remains unclear. Therefore, this study takes the Moziping Tunnel exit section of the Kaiyun Expressway in Chongqing as the engineering background. A combination of theoretical analysis, numerical simulation, and field monitoring is employed to investigate the impact of shallowly buried, oblique tunnel portal excavation on the stability of soil–rock layered slopes at the tunnel portal. First, this study establishes a mechanical model for tunnel–soil–rock layered slopes, develops a layered stress transfer analysis framework, and proposes a stability evaluation method based on the transfer coefficient method. Second, discrete element software is used for numerical simulation, and the validity of the numerical results is verified by comparing them with field monitoring data. This further reveals the influence of portal excavation on the stress and deformation of soil–rock layered slopes and tunnels during the excavation process. Finally, by comparing the slope stability coefficients obtained from numerical simulations and theoretical calculations, the accuracy of the proposed computational theory is quantitatively validated. This study provides a theoretical basis for evaluating slope stability and disaster prevention in tunnel portal excavation under similar geological conditions.

Engineering background

This paper focuses on the exit section of the Moziping Tunnel in the Kaiyun Expressway, Chongqing, China. The tunnel exit is located in Yunyang County, Chongqing Municipality. The topographic location is shown in Fig. 1. The tunnel portal section is located in broken and weathered strata, with complex geological conditions, shallow buried and biased terrain, and a natural stream gully on the outer side of the slope, which is let down to a slope of 42°.

The upper cover of the slope is silty clay, and the lower bedrock is sandy mudstone and sandstone from the Penglai Township Formation, as shown in Fig. 2a. The specific geotechnical physical and mechanical property parameters are shown in Table 1. According to the rock mass classification for rock slopes, the slope rock mass is classified as Type III. The engineering safety level of the slope is classified as Level I. The slope is classified as Class II. Portal excavation disturbances in slopes promote the development of weak-level shear zones, which can lead to slip instability along the rock–soil interface at the toe of the slope and may further lead to deformation and damage to the tunnel lining structure. The casting set of arches is constructed by reserving core soil in the ring guide pit, and after entering the hole, it is excavated via the step method, with a step length of 10 m. After the difficulty of entering the right hole was analyzed, the left hole was excavated first. The slope stabilized during the excavation of the left hole. After 100 m of tunnel advance in the left portal, the slope of the portal was restabilized. The second lining support was poured into the left portal before the boring of the right tunnel started. The right tunnel intersects the soil and rock face, and excavation disturbances may create bedded landslides, affecting tunnel safety. A schematic cross-section of the tunnel portal is shown in Fig. 2b.

The construction area of the Moziping Tunnel is in a subtropical monsoon warm–humid climate zone characterized by mild and humid weather, abundant rainfall, and distinct seasonal temperature variations. The portal construction monitoring period was during the winter and spring, with relatively low rainfall. Atmospheric precipitation is the main source of groundwater recharge, and the tunnel is located above the groundwater table.
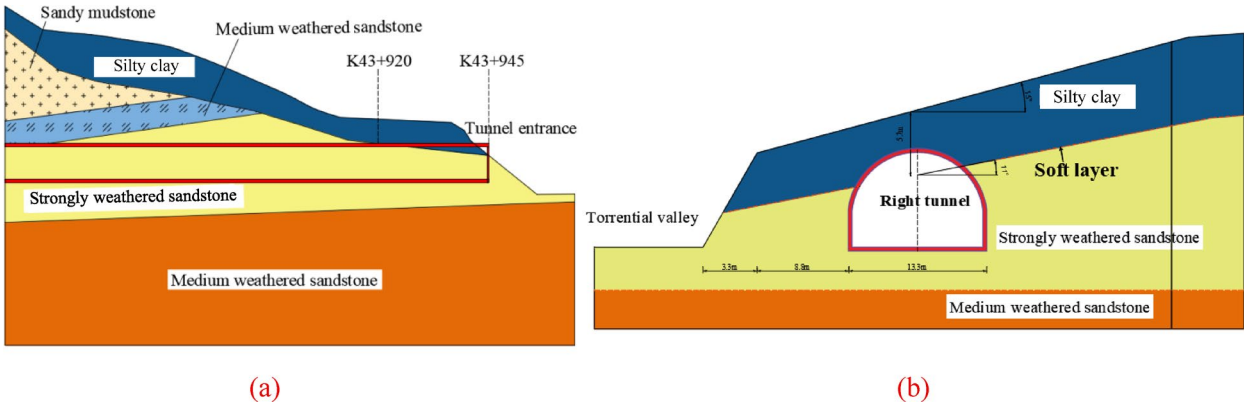
Fig. 1. Topographic location of the tunnel site.

(a)   (b)

Fig. 2. Geology of the road tunnel in longitudinal section and cross-section of the portal. (**a**) Geology of the tunnel in longitudinal section, (**b**) Cross-section of the portal.

Stratum Lithologic	Modulus of deformation (MPa)	Density (g/cm³)	Characteristic value of foundation bearing capacity f_{a0} (kPa)	Cohesion c (kPa)	Angle of internal friction φ (°)
Silty clay	4.4	1.95	140	23.5	12
Sandy mudstone	22	2.06	280	35	22
Strongly weathered sandstone	25	2.1	300	45	25
Medium weathered sandstone	3551	2.45	1500	1500	35

Table 1. Physical and mechanical parameters of geotechnical properties.

Stability analysis method for soil–rock bedding slopes under tunnel portal excavation disturbances

Calculation model of tunnel–soil-rock bedding slopes

Tunnel excavation will cause damage to the surrounding rock at the side slopes. Excavation unloading causes the soil column above the tunnel to sink and transmit force to the surrounding rock on both sides. When the force exceeds the strength of the rock and soil, it will cause cracks in the soil body until it extends to the surface and affects the sliding force of the slider. On the basis of engineering geological conditions and existing theoretical failure models of tunnel portal slopes, a computational model for soil-rock bedding slopes under the disturbance of tunnel portal excavation is established for shallowly buried bias tunnels, as shown in Fig. 3.
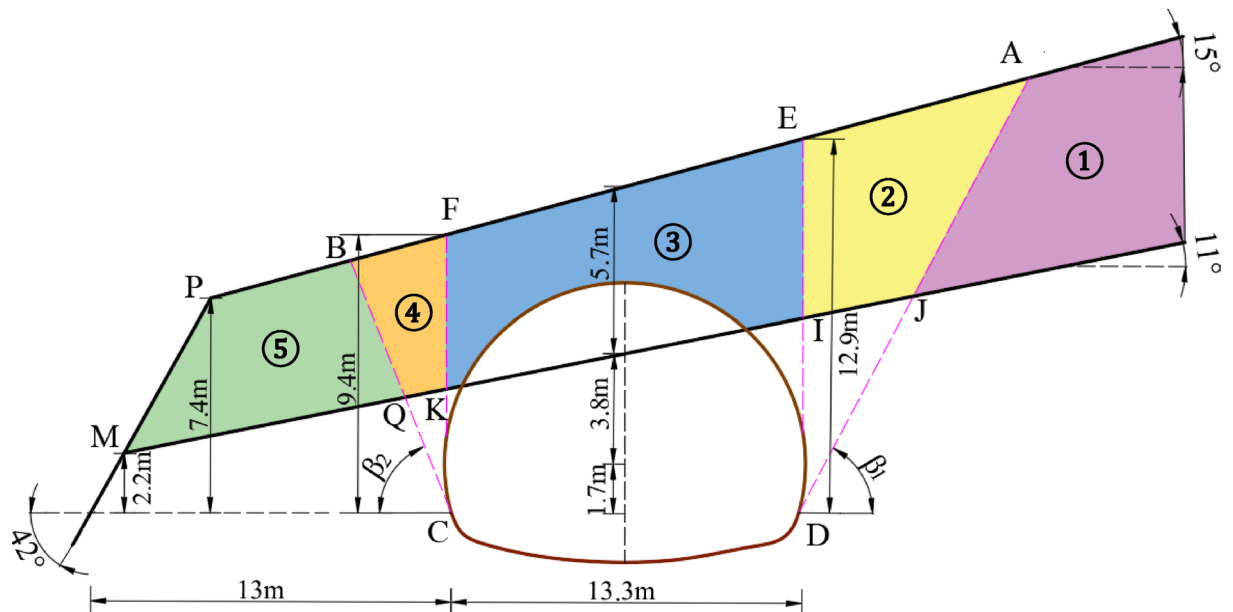
Fig. 3. Calculation model of the tunnel-soil-rock bedding slope.

The disturbance of tunnel excavation leads to damage to the surrounding rock on both sides, and the cracks AD and BC extend to the surface. Owing to the influence of bedding structure, the upper soil layer clearly tends to slide. In addition, owing to the thinness of the upper soil layer, the unloading caused cracks at the FK and EI. To further assess slope stability, it is necessary to clarify the specific location of surrounding rock damage, analyze the force state of the sliding body, and calculate the soil-rock bedding slope safety coefficient.

The overlying strata of the tunnel are stockpiled soils, the bedrock is strongly weathered sandstone, o is the level dip, and α is the slope dip. The strata at the tunnel portal are broken and weathered, with little difference between the softness and hardness of the stockpiled soil and the strongly weathered sandstone. The rupture surface formed by the disturbance is simplified as a straight line, and the weighted average of the combined stratigraphic parameters determines the rupture angle. The different strata in the loosening zone are kept in equilibrium separately, and the safety factor for the soil and rock faces is calculated. Excavation disturbances and pressure distributions in soil and rock strata must be studied and clarified. The longitudinal 1 m length of the tunnel is taken for the study so that the 3D structure can be transformed into a 2D model for analysis. Since the tunnel is orthogonal to the level, the vault soil body ③ is supported by the lining structure after excavation and sinking and is relatively stable. The loose soil on both sides remains stable and resists the sliding of the vault soil, and vault soil ③ can also be stabilized. The soil-rock bedding slope is in a stabilized state in the natural state. After excavation, the unloosened soil ① on the deep buried side is squeezed by the loosened soil along the rupture surface, and the unloosened soil ① on the deep buried side is more conducive to stabilization than the natural state. After excavation, the loose soil ② on the deeply buried side changes. However, loose soil ② on the deeply buried side is subjected to the antislip effect of the intermediate soil and the supporting structure, and the possibility of instability is small. The center column compressed the loosened soil ④ on the shallow buried side, pushing the unloosened soil ⑤ on the shallow buried side. The shallow buried soil bodies ④ and ⑤ are at the foot of the slope and are more likely to be destabilized and landslide along the level at the foot of the slope.

For ease of calculation, the following assumptions are made about the process of calculating the factor of safety for tunnel-soil-rock bedding slopes:

(1) The rock and soil bodies around the tunnel are homogeneous, continuous, and isotropic and obey the Mohr-Coulomb yield criterion.

(2) On the basis of the study of Liu et al.[37] on the stresses in the surrounding rock of the combined formation, the composite formation simplifies the rupture surface formed by the disturbance to a straight line. The angle of rupture in homogeneous strata is derived from the force equilibrium of the loosened soil in the limit state, and the same applies to composite strata. The different strata in the loosened zone are balanced separately. The stratigraphic parameters of the weathered and fractured zones at the tunnel portal are weighted to obtain the failure angle β_2 for the shallowly buried side and the failure angle β_1 for the deeply buried side.

$$\tan \beta_2 = \tan \varphi + \sqrt{\frac{(1 + \tan^2 \varphi)(\tan \varphi + \tan \alpha)}{\tan \varphi - \tan \theta}} \tag{1}$$

where φ is the friction angle of the soil (°).

(3) A landslide mass is an ideal rigid-plastic material without deformation. Once the shear stress along the sliding surface reaches its shear strength, the landslide mass begins to experience shear failure along the sliding surface.

Analysis of slider forces on soil–rock bedding slopes

During the excavation of the shallowly buried bias tunnel at the portal, the soil–rock bedding slope generally remains stable, with the loose soil–rock mass maintaining its integrity and experiencing uniform stress. The upper soil layer poses a risk of bedding landslides. The upper soil slider ④ in the shallow buried lateral loosening zone of Fig. 3 is taken as the object of study, and its force schematic is shown in Fig. 4. It is subjected to the boundary sliding thrust, gravity, force with slider ⑤ and force at the level. Block ③ is stable and immobile, and the downward sliding thrust on slider ④ is F_0. F_0 is obtained according to the damage mode of the slope enclosure in the combined stratum[20]:

$$F_0 = \frac{1}{2}\gamma_1 \overline{FK}^2 \frac{\lambda_{21}}{\cos\theta_1} \tag{2}$$

where F_0 is the force between the upper soil and the intermediate column in the loosening zone on the shallow buried side of the bedding slope (kN/m); λ_{21} is the coefficient of lateral pressure of the upper soil layer on the shallow buried side of the bedding slope; γ_1 is the gravity of the soil above the bedding slope (kN/m³); and θ_1 is the friction angle of the upper layer of soil at the edge of the bedding (°).

$$\lambda_{21} = \frac{\tan\beta_2 - \tan\varphi_1}{\tan\beta_2 - \tan\alpha} \cdot \frac{1}{1 + \tan\varphi_1 \tan\theta_1 + (\tan\varphi_1 - \tan\theta_1)\tan\beta_2} \tag{3}$$

$$N_1 = W_3 \cos o + F_0 \sin(\theta_1 - o) \tag{4}$$

$$T_1 = c_1 l_1 + N_1 \tan\varphi_1 \tag{5}$$

$$F_1 = W_3 \sin o + F_0 \cos(\theta_1 - o) - (c_1 l_1 + N_1 \tan\varphi_1)/F_s \tag{6}$$

where W_3 is the self-weight of slider ④ (kN/m); N_1 is the normal force at the level of slider ④ (kN/m); T_1 is the anti-slip force of slider ④ (kN/m); F_1 is the residual downward sliding force of slider ④ (kN/m); c_1 is the cohesive force of the soil in the upper layer of bedding slope (kN/m²); l_1 is the length of the bottom of slider ④ (m); o is the level angle of inclination (°); F_s is the safety factor of the slope; and φ_1 is the internal friction angle of the upper soil layer of the bedding slope (°).

The upper soil slide ⑤ in the shallowly buried side loosening zone of Fig. 3 is taken as the object of study, and its force schematic is shown in Fig. 5. It is subjected to gravity, the remaining sliding force of slider ④ and the force at the level.

$$N_2 = W_4 \cos o \tag{7}$$

$$T_2 = c_1 l_2 + N_2 \tan\varphi_1 \tag{8}$$

$$F_2 = W_4 \sin o + F_1 - (c_1 l_2 + N_2 \tan\varphi_1)/F_s \tag{9}$$

where W_4 is the self-weight of slider ⑤ (kN/m); N_2 is the normal force at the level of slider ⑤ (kN/m); T_2 is the anti-slip force of slider ⑤ (kN/m); F_2 is the residual sliding force of slider ⑤ (kN/m); and l_2 is the length of the bottom of slider ⑤ (m).

When the slope stability factor is calculated via the transfer coefficient method, the shear strength parameters (cohesion c and internal friction angle φ) must be iteratively reduced until the slope reaches the limit equilibrium state.
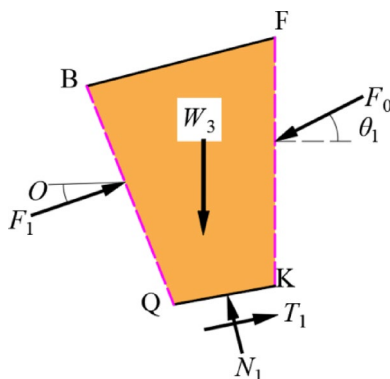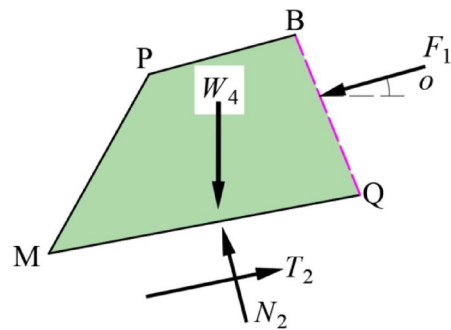

Fig. 4. Schematic diagram of the force on slider ④.

Fig. 5. Schematic diagram of the force on slider ⑤.

Rock−soil mass	Gravity γ kN/m³	Force of cohesion c/Pa	Angle of internal friction φ/°
Silty clay	19.5	23,500	12
Strongly weathered sandstone	21	45,000	25

Table 2. Rock and soil parameters of the tunnel exit slope.

$$c' = \frac{c}{F_s} \tag{10}$$

$$\tan \varphi' = \frac{\tan \varphi}{F_s} \tag{11}$$

where c' represents the reduced cohesion, φ' represents the reduced internal friction angle, and F_s is gradually increased from the initial value of 1.0, ensuring that the reduction process is systematic rather than random.

Iterative adjustment process:

(1) Initial assumption: Set the initial reduction coefficient F_s and calculate the remaining sliding force F_i for each soil layer.
(2) Convergence judgment: If the remaining sliding force of the last soil layer $F_n > 0$, the current F_s is too small, and F_s should be increased to increase the reduction strength. If $F_n < 0$, F_s should decrease.
(3) Optimization calculation: To accelerate convergence, numerical optimization methods such as the bisection method can be used to adjust F_s until F_n approaches the preset tolerance.
(4) Result determination: When $F_n = 0$, the corresponding value of F_s is the slope stability safety factor.

Calculation of slope safety coefficients for soil–rock bedding after tunnel excavation disturbance

The tunnel portal intersects with the soil‑rock bedding slope, and the excavation disturbance aggravates the instability risk of the natural potential slip zone (soil and rock surface). It is necessary to quantitatively evaluate the safety factor of a slope after excavation. The calculated length parameters of the model are shown in Fig. 3. The physical and mechanical parameters of the rock and soil samples obtained via geological surveys and laboratory tests are shown in Table 2. The safety factor of the soil‑rock bedding slope of the tunnel is calculated according to Eqs. (1)–(10). After calculation, the fracture angle β_2 of the shallow buried side is 61°, and the lateral pressure coefficient of the upper soil on the shallow buried side of the tunnel is 0.77. Through several iterations of calculation, the slope safety coefficient after excavation construction is obtained as 1.18, which is 27% lower than that before excavation. Although the slope safety coefficient is greater than 1, its value is close to the limit state, indicating that the risk of landslides at the foot of the slope is high.

The slope at the exit of the Moziping tunnel is composed of accumulated soil and strongly weathered sandstone, and the layer is orthogonal to the tunnel. The strength of the accumulated soil and soil rock surface is very low, the burial depth of the tunnel entrance is shallow, and the terrain is biased. The above factors constitute the primary triggers of slope deformation during excavation. On the basis of the site conditions, deformation occurred mainly in the upper stockpile soil, whereas bedrock deformation was more minor. During excavation, the upper soil layer in the arch top and arch shoulder areas sinks faster. This is due to the thinness and low strength of the overlying soil layer, which leads to the limited role of the load-bearing arch in excavation and the inability to effectively resist ground pressure. In addition, the slopes have weak structural surfaces, and the ground pressure is transferred to the soil and rock surfaces when the upper soil subsides and slips. Owing to the high strength of the bedding, the bedding structure causes the soil in the upper part of the tunnel to slip along the level to the adjacent side, which in turn causes damage to the surrounding rock and cracks. The cracks produced by damage to the surrounding rock of the soil‑rock bedding slope are shown in Fig. 6.

The deformation and displacement of the slope are large at the top of the arch and the shoulder of the arch. During tunnel excavation unloading, the soil column above the tunnel sinks while force is applied to the soil on
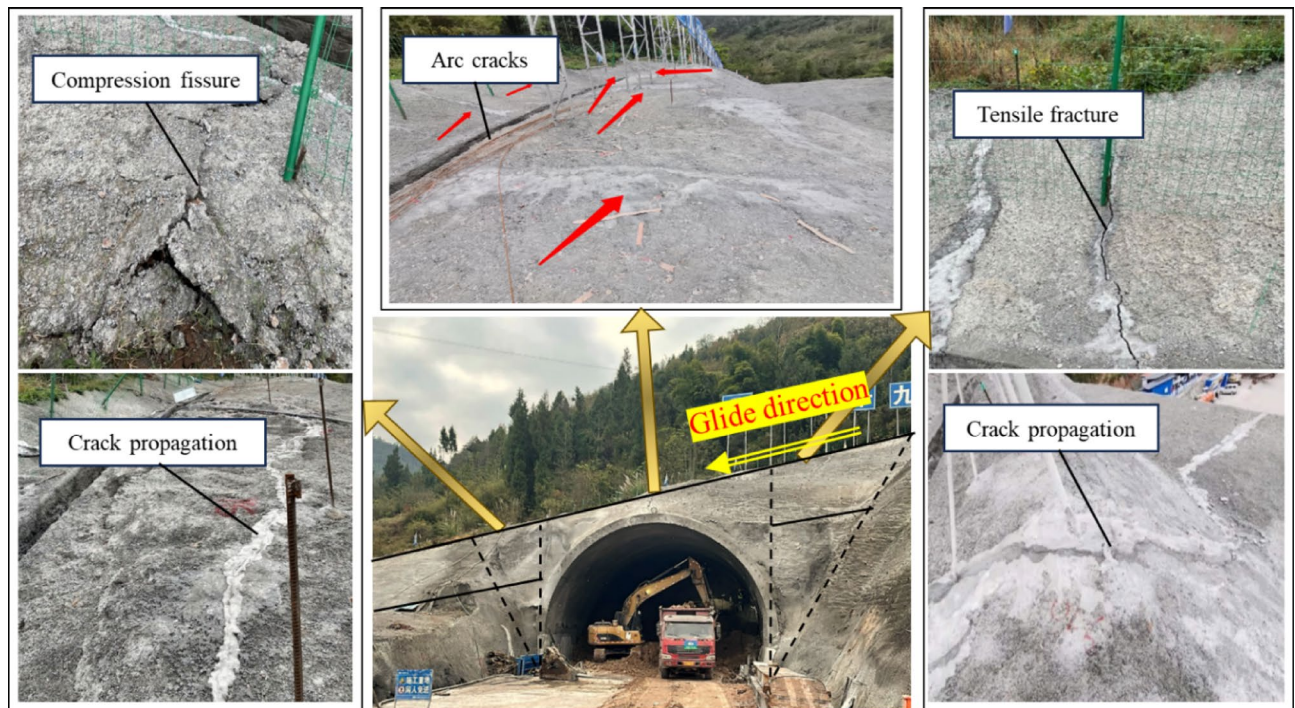
Fig. 6. Comparison and analysis of the theoretical calculation model and field conditions.

both sides. The soil on both sides of the tunnel squeezes into the tunnel, causing cracks in the surrounding rock until it extends to the surface. The soil at the vault has poor self-stabilizing ability. The bedding structure makes the sliding of the soil at the upper part of the tunnel drive the trailing edge of the slope and push the leading edge of the slope to slip slowly along the surface to the free area. Thus, the displacement monitoring data at the surface and soil–rock junction are significantly larger than the bedrock displacement monitoring data. This also corresponds to the relative stability of the front and rear edges of the slope, with the vault and arch shoulders experiencing significant settlement, forming a settlement trough. In addition, arcuate cracks appeared above the tunnel, formed by slumping soil at the top of the arch protruding into the back edge of the side slopes. Tension cracks appeared at the trailing edge of the slope, the formation mechanism of which was mainly due to the extrusion of the tunnel by excavating the soil on the deeply buried side. The deformation of the right arch shoulder is significantly greater than that of the left arch shoulder, and this asymmetric deformation characteristic indicates that the tunnel structure assumed a role similar to that of a skidding pile, which effectively resisted the sliding of the soil at the trailing edge. The soil at the top of the arch slips and pulls the deeply buried side soil, and when the force exceeds the tensile strength of the soil, tension cracks are formed at the trailing edge of the slope. Moreover, the shear cracks at the leading edge of the slope continue to expand. After excavation and unloading, the shallowly buried side soil body stress is released. The extrusion effect of the soil body at the arch top is enhanced, which leads to arching of the ground surface and the formation of shear cracks at the foot of the slope along the slope, indicating that there is a risk of translational landslides along the level at the foot of the slope.

Stabilization was maintained after stopping, and stabilizing measures were taken at the site. Before construction excavation, the safety of soil–rock bedding slopes at the portal after excavation disturbance was evaluated according to the derived formula. Predicting the landslide risk caused by excavation is important for tunnel support design and slope management. The theoretical calculation model is compared and analyzed with field reality, and a comparison and analysis diagram is shown in Fig. 6. The monitoring results revealed that portal excavation caused large surface settlement and deformation of the tunnel vault and arch shoulder. When the shallow buried lateral arch shoulder is larger than the deep buried lateral arch shoulder is, the leading and trailing edges of the slope are relatively stable. This corresponds to the slope level safety factor obtained from theoretical calculations. The shallow buried side of the slope arch shoulder developed shear cracks and extended along the slope to the front edge, which was due to the shallow buried side of the loose area of the soil shear damage and extrusion shear unloosened soil, with the entire foot of the slope soil being close to the limit state. The anti-slip effect is exerted by the tunnel support structure, and the intervening soil stabilizes the loose soil on the deeply buried side. With the support structure intact, more can be done to mitigate compression on the shallow buried side and maintain stability on the deeper buried side. On-site slope deformation, monitoring result analysis and theoretical calculations coincide, and theoretical calculations before excavation can predict the excavation risk of the tunnel exit approach.

Numerical simulation and field monitoring

To verify the accuracy of the theoretical model and reveal the impact of tunnel portal excavation on the soil‒rock layered slope and the stress and deformation of the tunnel, this section adopts a verification method that combines numerical simulation and field monitoring. The specific research process is shown in Fig. 7. First, the numerical model is validated for effectiveness on the basis of field monitoring data. Second, numerical simulations are used to analyze the impact of the entire tunnel portal excavation process on the soil‒rock layered slope and the stress and deformation of the tunnel. Finally, the stability coefficient of the slope obtained from the numerical simulation and theoretical calculations is compared to achieve quantitative verification of the accuracy of the computational theory.

Modeling of finite difference methods

On the basis of the design parameters and construction methods of the Moziping Tunnel Project, FLAC3D software is used to numerically simulate and analyze slope stability during tunnel excavation. The Mohr‒Coulomb criterion is chosen for the constitutive model of the geotechnical body. In the model, the soil‒rock surface and the surrounding rock are continuous and isotropic elastic‒plastic bodies along the interface direction, and the calculation process is carried out according to the Mohr‒Coulomb criterion. Only the stress field caused by the self-weight of the model is considered in this simulation. In the model, the negative direction of the Z-axis is the direction of gravity, and the positive direction of the Y-axis is the direction of tunnel excavation. The calculations do not consider the effects of groundwater seepage. On the basis of the length parameters such as tunnel cross-section size and tunnel burial depth in the design data of the Moziping Tunnel, as well as the physical and mechanical parameters of the ground layer and the supporting structure, a numerical model is established via FLAC-3D software, as shown in Fig. 8. The net height of the tunnel H = 9.1 m, the net width of the tunnel B = 13.3 m, and the clear distance of the tunnel is 22 m. The dimensions of the numerical model in the Y direction are 55 m, the distance from the bottom boundary to the tunnel is 30 m, and the distance from the left and right boundaries to the neighboring tunnels is 40 m.

The temporary support adopts steel arch frames and shotcrete. The elastic modulus of the steel arch frame is equivalent to that of the concrete to simplify the modeling process of the steel arch frame and the calculation model. The specific conversion method is as follows:

$$E'_h = E^0_h + A_g E_g / A_h \tag{12}$$

where E'_h, E^0_h, and A_g represent the elastic modulus of the converted concrete, the original elastic modulus of the concrete, and the cross-sectional area of the shotcrete, respectively, and where E_g and A_g represent the elastic modulus and cross-sectional area of the steel arch frame, respectively.

According to the engineering geological conditions and design scheme of the exit of the Moziping Tunnel, the physico-mechanical calculation indices needed for this numerical simulation are shown in Table 3.

The tunnel is excavated via the benching method. Owing to the shallow burial and poor conditions of the portal slope, mechanical excavation is adopted for the portal. The excavation process in the model is consistent with the actual construction conditions. The left tunnel reaches 100 m, and the second lining at the portal is cast before proper tunnel excavation begins. Additionally, since the left tunnel at the portal is far from the slope toe, the excavation of the left tunnel has a negligible impact on the portal slope. Therefore, the simulation focuses on the excavation process of the right tunnel and its impact on the portal slope. In the model, the longitudinal dimension of the right tunnel is 55 m, and the excavation process follows a step-by-step approach, with each excavation cycle being 2 m long.

Monitoring point layout

The layout of the initial support monitoring points for both the engineering monitoring site and the numerical simulation is shown in Fig. 9a and b. Among them, point A is the settlement measuring point of the tunnel vault, BC is the convergence measuring line around the upper step, and DE is the convergence measuring line around the lower step. The upper step monitoring point is in the accumulated soil, and the lower step monitoring point is in the bedrock. The surface monitoring points were arranged as shown in Fig. 9c and d and were distributed on
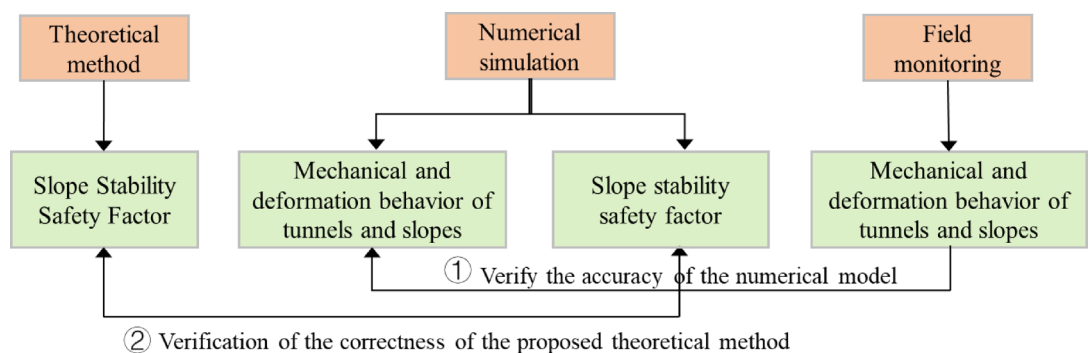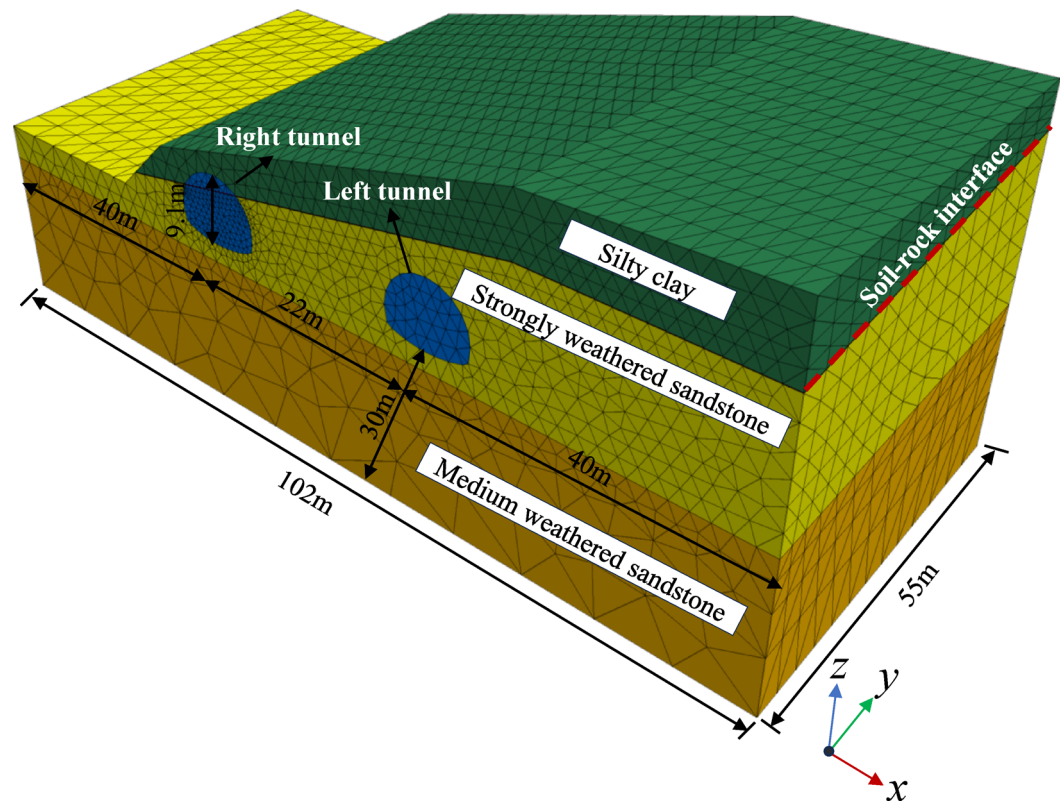

Fig. 7. Specific research process.

Fig. 8. FLAC3D 3D numerical model.

Rock–soil mass	Elastic modulus E (Pa)	Poisson's ratio v	Gravity γ (kN/m³)	Cohesion c (Pa)	Internal friction angle φ (°)
Silty clay	2.2×10^7	0.29	19.5	23,500	12
Strongly weathered sandstone	1.25×10^8	0.35	21	45,000	25
Medium weathered sandstone	1.7×10^{10}	0.31	24.5	1,500,000	35
Initial support	2×10^{10}	0.2	24	/	/
Secondary lining	2.5×10^{10}	0.2	25	/	/

Table 3. Physical and mechanical parameters of geotechnical bodies in the computational simulation.

the slope above the portal. The first three monitoring sections of the cave corresponded to the surface monitoring sections.

Results analysis

Deformation characteristics of the slope after the initial excavation of the left tunnel
The contour maps of the vertical displacement, horizontal displacement, and plastic strain of the slope after excavation of the left tunnel are shown in Fig. 10. As shown in Fig. 10a and b, the excavation of the left tunnel has a minimal impact on the displacement of the soil-rock layered slope. The maximum vertical and maximum horizontal displacements are only 6 mm and 3 mm, respectively. As shown in Fig. 10c, the plastic deformation induced by the excavation of the left tunnel is primarily concentrated around the tunnel perimeter, with minimal impact on the plastic deformation of the slope. This is primarily because the left tunnel is located in deeply buried, intact bedrock, where the geological conditions are relatively stable. In conclusion, the impact of left tunnel excavation on the failure mode of the soil-rock layered slope is minimal. Therefore, the influence of the left tunnel was not considered when establishing the soil-rock layered slope failure model in this study. As a result, after the excavation of the left tunnel, the effects it caused were nullified in the simulation.

Displacement characteristics of the slope during excavation of the exit right tunnel
The exit of the Moziping Tunnel is shallowly buried and biased, and the portal is orthogonal to the soil and rock surface. To fully reveal the deformation law of slopes in the excavation process, cross sections K43 + 925 and K43 + 915, which are located in the soil-rock stratum and bedrock stratum, respectively, are selected as the research objects. The vertical displacement and horizontal deformation corresponding to the two sections are shown in Figs. 11 and 12. By comparing and analyzing the deformation characteristics of the slopes in these two sections
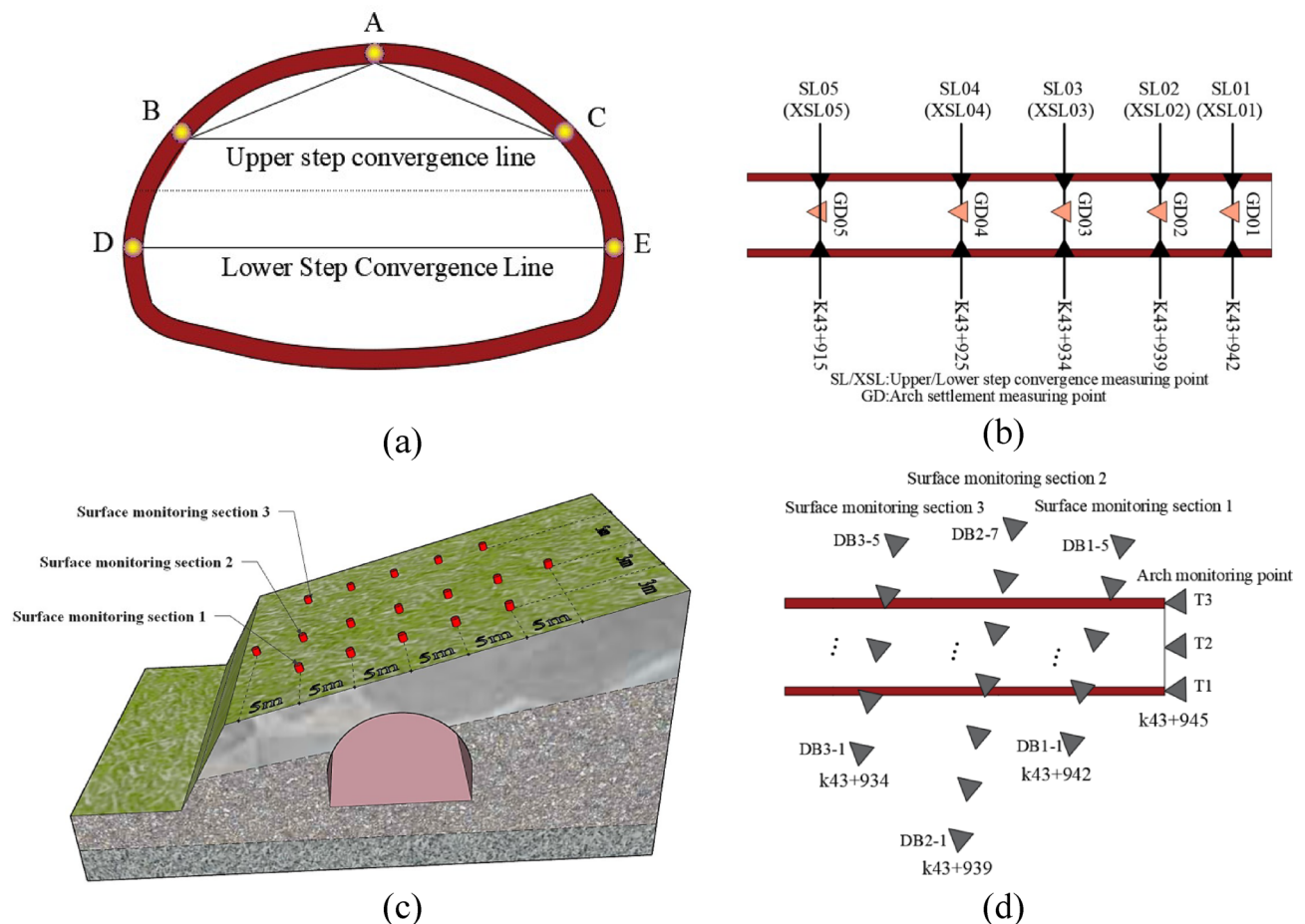
Fig. 9. Layout of the monitoring points. (**a**) Arrangement of tunnel arch settlement and perimeter convergence measurement points, (**b**) monitoring section inside the tunnel, (**c**) distribution of surface measurement points, and (**d**) top view of surface measurement point locations.

during the excavation process, the deformation laws of the soil-rock bedding slopes and their characteristics are summarized. The vertical displacement of the tunnel portal slope and the vertical displacement distribution on the longitudinal section at the K43 + 925 section during tunnel excavation are shown in Fig. 11a and b. Larger values of vertical displacement on the tunnel axis occur at the portal, where the soil in the upper part of the portal vault is at the boundary. Poor arching effect of thinner soils under excavation unloading. The surface settlement at section K43 + 945 is 36 mm. Section K43 + 925 is 10 mm long, and section K43 + 915 is 2.5 mm long. The displacement in the X direction differs between the soil and rock layers, with a more significant variation at the toe of the slope and a risk of sliding along bedding planes. Owing to the support provided by the tunnel lining structure, the X-direction deformation remains consistent across the layers on the deeply buried side of the tunnel. The vertical displacement of the tunnel portal slope and the vertical displacement distribution on the longitudinal section at the K43 + 915 section during tunnel excavation are shown in Fig. 11c and d. The continued excavation of the tunnel has a limited effect on the deformation at the portal. The surface settlement monitoring data reveal that the surface settlements of the K43 + 945, K43 + 925 and K43 + 915 sections on the tunnel axis are 37.3 mm, 17 mm and 8 mm, respectively, with the change amplitude increasing by 3.6%, 70% and 220%, respectively, which indicates that the settlement shows significant spatial variability with the change in section location. Further analysis reveals that the deformation of the surrounding rock gradually decreases as the tunnel excavation position moves away from the portal; when the tunnel enters the bedrock stratum, the quality of the surrounding rock improves significantly, and the deformation caused by the excavation is further reduced, whereas the integrity of the supporting structure is gradually enhanced, and the overall stability is significantly improved. The variation in horizontal displacement is minimal. After the tunnel reaches the bedrock, the surrounding rock mass improves, and the deformation during excavation gradually decreases. As the support structure becomes more complete, the overall stability improves.

To study the influence of tunnel excavation on the slope stability of soil-rock bedding at the portal in detail, for the characteristics of large deformation in the portal area, the surface monitoring points corresponding to the field measurements of section K43 + 942 of the Moziping Tunnel in the numerical model and the monitoring points inside the cave are selected for comparison and analysis. The displacement data obtained from the simulation of each monitoring point of the K43 + 942 section were extracted, and the curves of the simulated
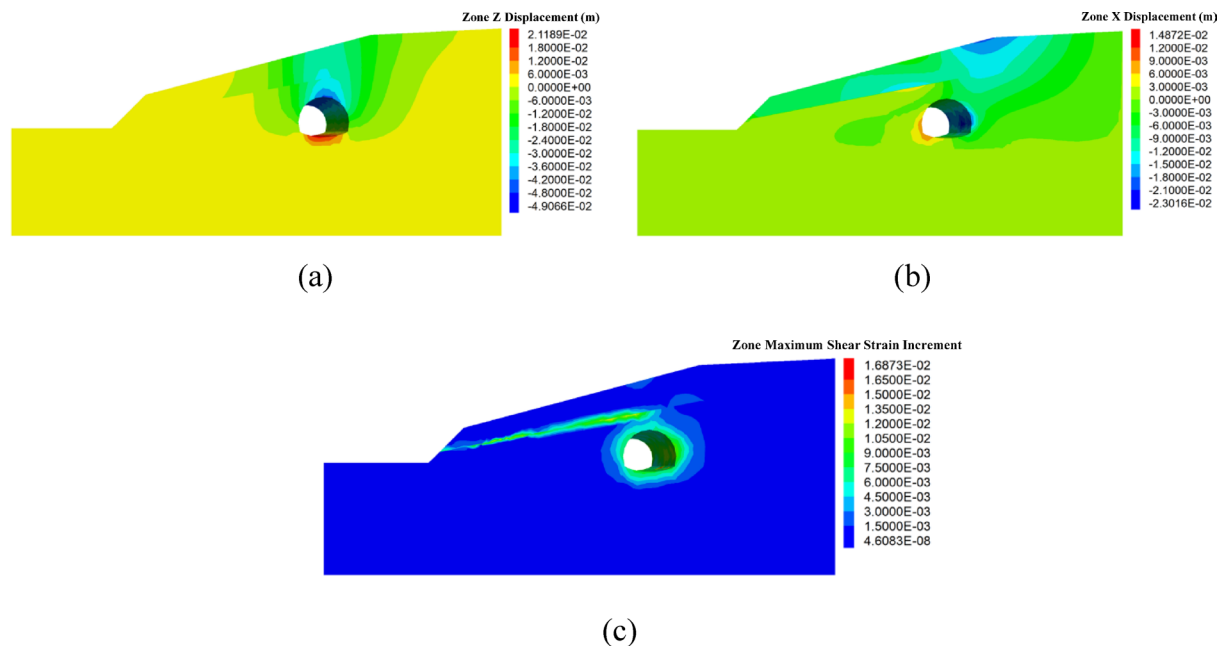
(a)

(b)

(c)

Fig. 10. Deformation and plastic strain contour plots of the slope after the excavation of the left tunnel. (**a**) Vertical displacement, (**b**) horizontal displacement, and (**c**) plastic strain.

and measured values of the displacement of the measuring points with the change in tunnel excavation were plotted, as shown in Fig. 13.

This can be seen by analyzing the displacement graphs of each monitoring point in the numerical simulation:

(1) The effects of the tunnel excavation distance on the settlement of the portal slope, crown settlement, and tunnel convergence can be divided into three stages. Stage I is the rapid deformation stage, which mainly occurs during the excavation of the tunnel portal. When the tunnel excavation distance reaches 0.22D (where D is the tunnel width), significant changes are observed in all monitored parameters: the maximum surface settlement of the slope reaches 25 mm, accounting for 78.1% of the total cumulative settlement; the peak crown settlement reaches 30 mm, accounting for 81.1%; and the maximum tunnel convergence reaches 22 mm, accounting for 68.92%. Stage II is the slow deformation stage (with the excavation distance ranging from 0.22D to 2.63D), characterized by a significant reduction in the deformation rate after the tunnel face passes the monitored section. Moreover, partial rebound of the crown settlement and tunnel convergence are observed, which is attributed to the support structure beginning to play a role in stabilizing the tunnel. Stage III is the stable development stage (when the excavation distance exceeds 0.63D), during which the rate of change in all monitored parameters gradually approaches zero as the tunnel face moves farther from the monitored section, ultimately reaching a stable state.

(2) The numerical simulation results reveal that the settlement at the crown and shoulder of the arch is relatively large, with excavation unloading causing significant deformation in the thin soil layer at the tunnel top. The tunnel convergence simulated for the upper step is greater than that for the lower step, and there are differences in the horizontal displacement between the layers.

(3) A comparison between the numerical simulation results and the field monitoring data indicates that the trends of slope settlement, tunnel crown settlement, and tunnel convergence are generally consistent, validating the reliability of the numerical simulation model. Among these values, the monitored values of crown settlement and tunnel convergence are slightly smaller than the simulated values, which is attributed to the fact that the tunnel face had just been excavated onsite. Processes such as mucking and shotcreting delay the installation of monitoring equipment, resulting in a lag in the displacement monitoring records compared with the simulation time.

Stability analysis of soil-rock bedding slopes
The stability of soil-rock bedding slopes at shallowly buried bias tunnel portals is analyzed via the strength discount method, and the results are compared with those of theoretical calculations. As shown in Fig. 14, after the excavation of the right tunnel, a significant plastic strain concentration occurs at the foot of the slope on the shallow bedding side, which is mainly distributed at the weak level and first induces bedded landslides. The slope safety coefficient obtained from the numerical simulation is 1.13, which is only 4% different from the theoretical calculation (the safety coefficient is 1.18), verifying the reliability of the theoretical calculation. Zooming the location of the larger plastic strain, as shown in Fig. 15, the plastic strain at the location of the arch shoulder of the shallow buried side of the right tunnel extends to the surface. This corresponds to the location of extrusion shear cracks in the field and is also consistent with the conclusion of the theoretical analysis that the
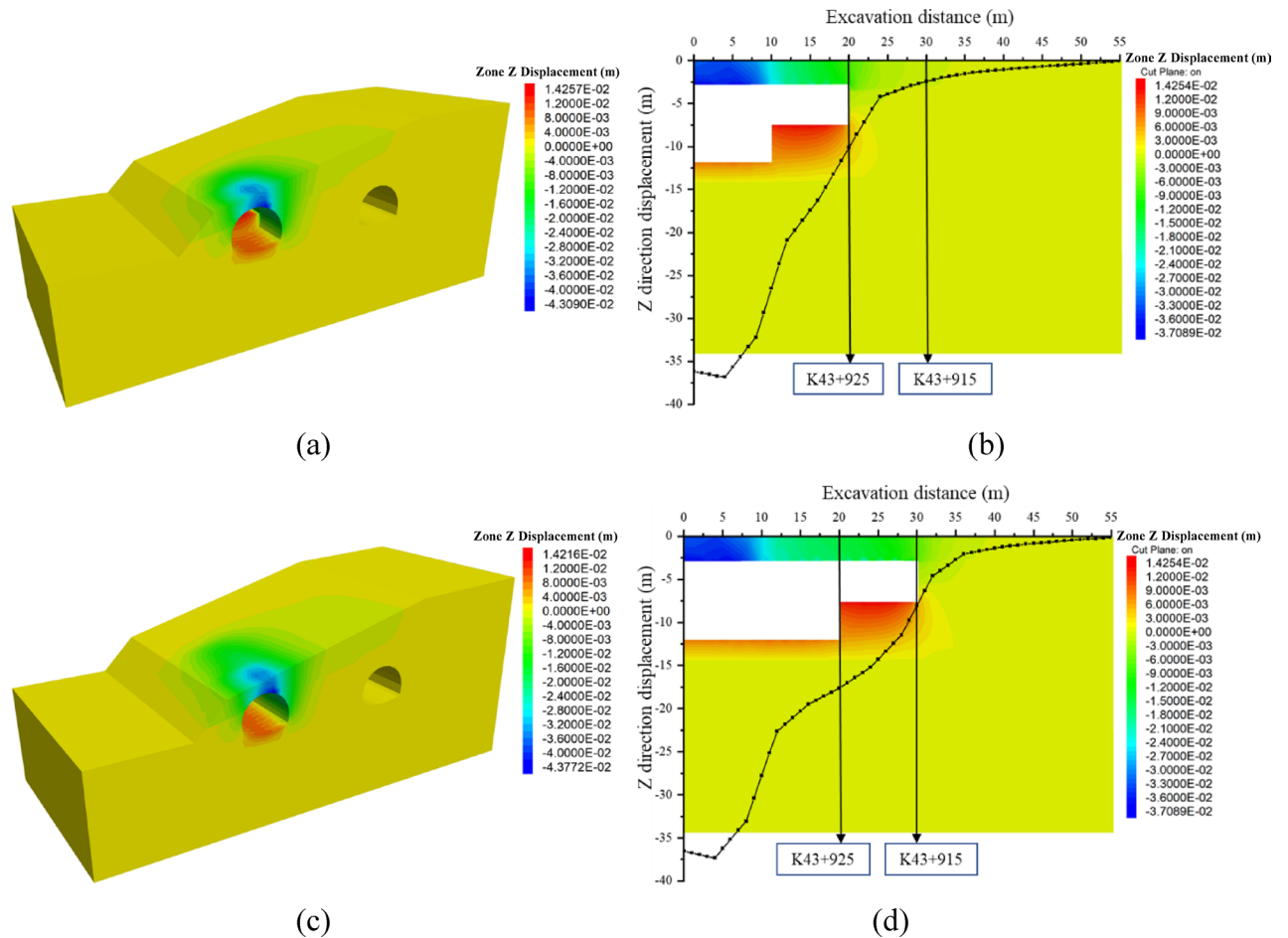
Fig. 11. Vertical displacement of the slope and surface under different excavation conditions. (**a**) Z-direction displacement of the portal slope in section K43 + 925, (**b**) vertical displacement of the surface in the l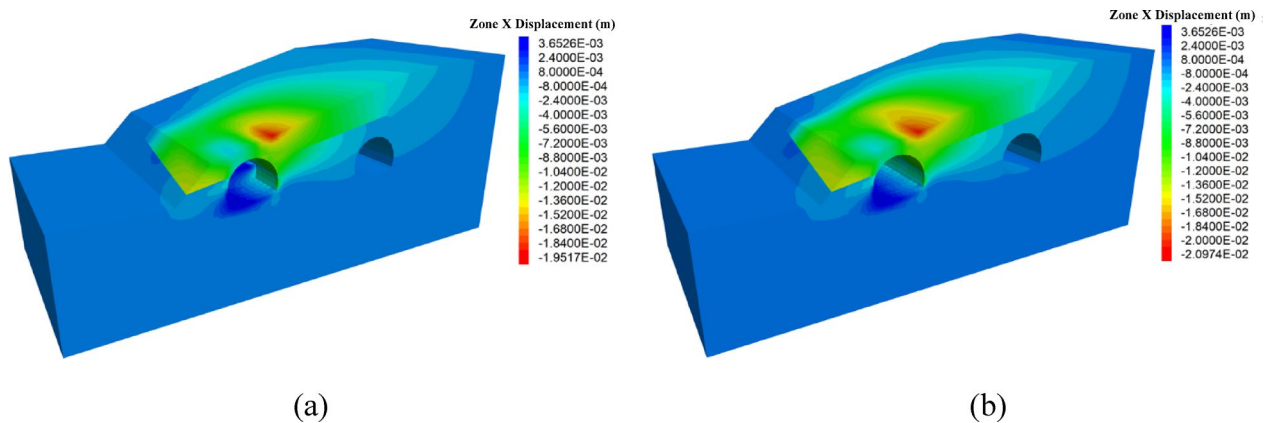ongitudinal section of the right tunnel in section K43 + 925, (**c**) Z-direction displacement of the portal slope in section K43 + 915, and (**d**) Z-direction displacement of the surface in the longitudinal section of the right tunnel in section K43 + 915.

Fig. 12. Displacement contour maps of the slope in the X direction at the K43 + 925 and K43 + 915 sections during tunnel excavation. (**a**) K43 + 925, (**b**) K43 + 915.
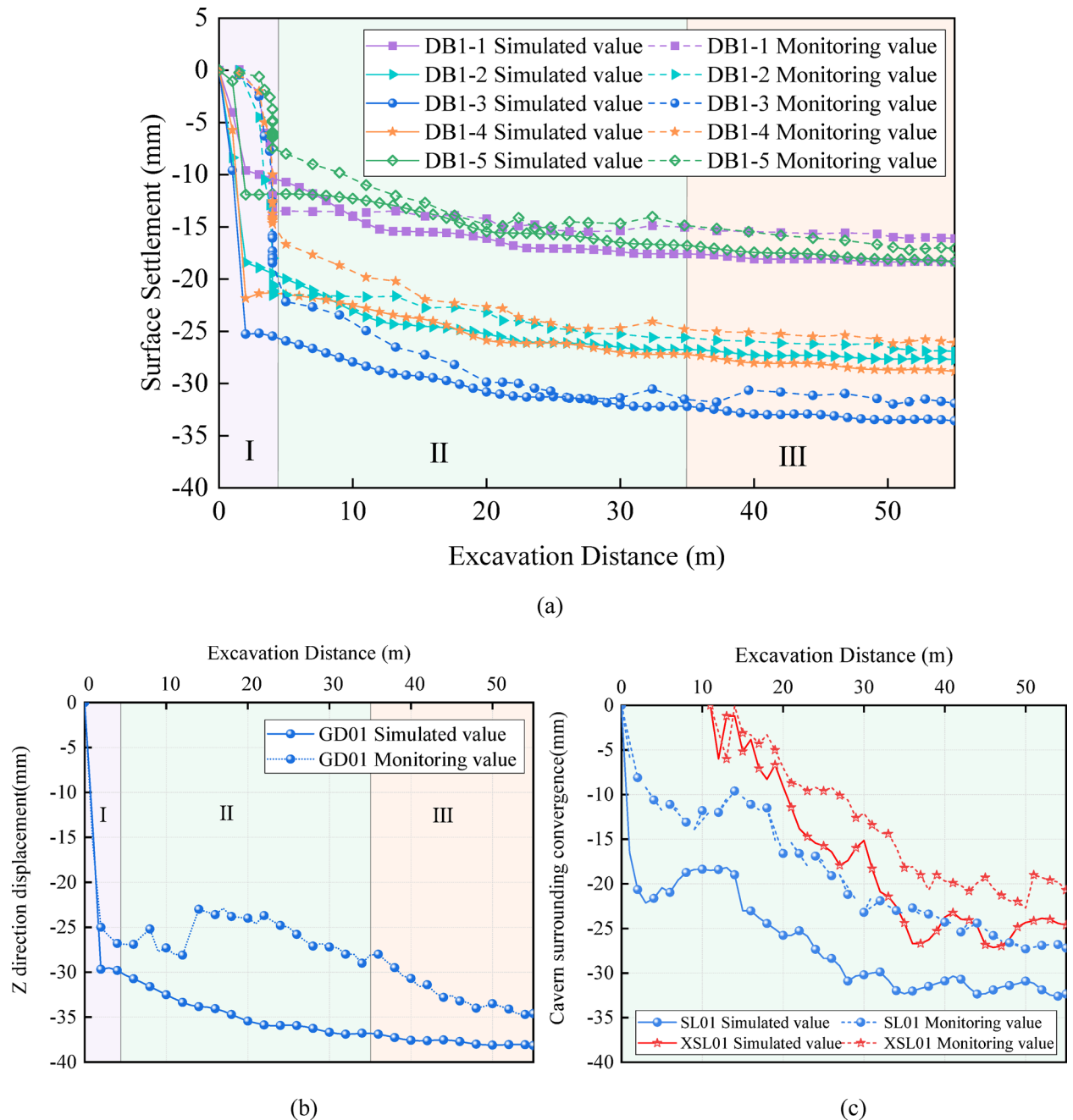
Fig. 13. Comparison of simulation and monitoring surface settlement, vault settlement and cave perimeter convergence at the K43 + 942 section. (**a**) Comparison of simulated and monitored surface settlement, (**b**) comparison of simulation and monitoring of vault settlement, (**c**) comparison of simulation and monitoring of cave circumferential convergence.

loosening zone of the shallow buried side is unstable. The loosened soil transfers stress to the unloosened soil, resulting in large plastic strains at the foot of the slope and affecting the stability of the entire foot. Intuitively, the bedded landslide is the weak point of the slope. In combination with factors such as the bedding structure, the intersection of the portal and the level, and the proximity of the tunnel portal to the toe of the slope, tunnel excavation results in a greater risk of bedded landslides along the level of the toe of the slope.

In summary, the weak bedding slope is the most dangerous location, which is consistent with the preconstruction slope stability prediction. After tunnel excavation, the foot of the soil-rock bedding slope at the portal has a greater landslide risk. The excavation disturbance causes the soil body at the foot of the slope to experience extrusion from the tunnel and the intermediate soil body. The plastic strain at the foot of the slope is greater, and the safety coefficient of the side slope is 1.13, which is close to the limiting equilibrium state. Owing to the anti-slip effect of the tunnel support structure, the plastic strain of the soil body on the deeply buried side is minor, which corresponds to the results of the theoretical analysis.
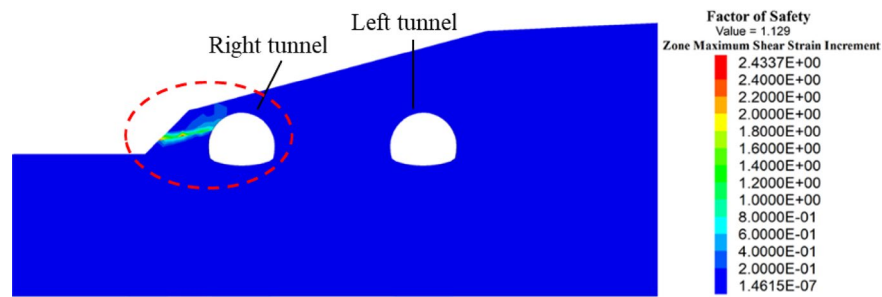
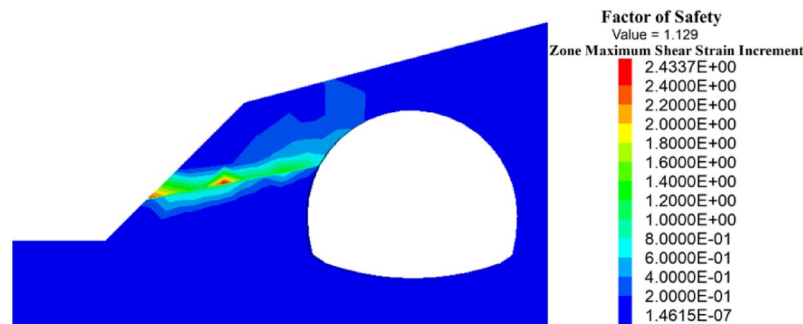**Fig. 14**. Plastic strain distribution of the portal slope under the original working conditions.

Fig. 15. Localized enlargement of plastic strain under the original working conditions.

Conclusion

This study uses the engineering background of the Moziping Tunnel exit section. This method employs a combination of theoretical analysis, numerical simulation, and field monitoring to systematically investigate the impact of shallowly buried and biased tunnel portal excavation on the stability of soil‑rock layered slopes. This study thoroughly reveals the deformation patterns and failure mechanisms of slopes. The main research conclusions are as follows:

(1) This study established a tunnel‑soil‑rock layered slope mechanical model based on the transfer coefficient method and developed a layered stress transfer analysis framework. Furthermore, a stability evaluation method suitable for soil‑rock layered slopes was proposed, addressing the limitations of traditional methods in handling composite strata. Theoretical calculations indicate that the slope stability factor decreases to 1.18 after excavation, significantly increasing the risk of landslides.

(2) The numerical simulation results closely agree with the field monitoring data, validating the model's accuracy. The simulated slope stability factor is 1.13, which is only a 4% difference from the theoretical calculation results, further confirming the reliability of the proposed method. In addition, the simulation revealed the concentration of plastic strain at the toe of the shallowly buried slope, corresponding to the location of shear cracks observed in the field, indicating that the toe is a potential slip zone.

(3) During the tunnel excavation process, the deformation of the slope and tunnel exhibits three distinct stages: a rapid deformation stage (excavation distance ≤ 0.22D), where the deformation accounts for 78.1–81.1% of the total deformation; a slow deformation stage (0.22D–2.63D), where the deformation rate decreases and is accompanied by partial rebound; and a stable stage (> 2.63D), where the deformation tends to stabilize.

(4) During tunnel excavation in a soil‑rock composite stratum, the overlying thin soil layer has poor self‑supporting capacity. It cannot form an effective bearing arch, leading to rapid soil deformation at the crown and arch shoulder areas after excavation unloading. Moreover, the interlayer slip effect at the soil‑rock interface induces significant horizontal displacement, causing compressive stress at the leading edge of the slope and forming a potential sliding plane. This results in the convergence of the surrounding rock in the upper step being significantly greater than that in the lower step. After reaching the complete bedrock section, the self-supporting capacity of the surrounding rock increases, the deformation induced by excavation disturbance significantly decreases, and the distribution becomes more uniform, leading to a rapid recovery of surrounding rock stability.

This study provides theoretical support for evaluating slope stability and disaster prevention during tunnel portal excavation under similar geological conditions. Future research can further explore the impact of dynamic construction techniques on slope stability.

Discussion

Although this study assumes that the sliding surface is a straight line and simplifies the landslide body as an ideal rigid-plastic material, comparison with actual monitoring data reveals that these simplifications have a relatively minor impact on the stability calculation results of the slope. The model's prediction results still accurately reflect the trend of changes in slope stability. However, given the complexity and uncertainty of different engineering scenarios, future research could further explore how to reduce the systematic errors introduced by these simplifications through more refined numerical models, thereby improving the accuracy and reliability of slope stability analysis.

Data availability

If someone wants to request the data from this study, please contact the author, Tao Li.

References

1. Meng, S. B. et al. Rapid resilience assessment framework for mountain tunnels subjected to near-fault seismic ground motions. *Soil Dyn. Earthq. Eng.* **182**, 108746 (2024).
2. She, Y. et al. Contribution of infrastructure to the township's sustainable development in southwest China. *Buildings* **12**(2), 164 (2022).
3. Jiang, L., Zhang, Q., Jia, C. J., Yu, J. & Huang, Q. F. Investigating on deformation characteristics and failure mechanism of bedding rock slope: Field study, long-term monitoring, and reinforcement measures. *Environ. Earth Sci.* **83**(2), 45 (2024).
4. Shi, S. S. et al. Intelligent prediction of surrounding rock deformation of shallow buried highway tunnel and its engineering application. *Tunn. Undergr. Space Technol.* **90**, 1–11 (2019).
5. Fan, G., Zhang, J. J., Wu, J. B. & Yan, K. M. Dynamic response and dynamic failure mode of a weak intercalated rock slope using a shaking table. *Rock Mech. Rock Eng.* **49**(8), 3243–3256 (2016).
6. Deng, Z. Y. et al. Model test and numerical simulation on the dynamic stability of the bedding rock slope under frequent microseisms. *Earthq. Eng. Eng. Vib.* **19**(4), 919–935 (2020).
7. Xu, B. T., Yan, C. H. & Xu, S. Analysis of the bedding landslide due to the presence of the weak intercalated layer in the limestone. *Environ. Earth. Sci.* **70**(6), 2817–2825 (2013).
8. Wang, D. P. et al. Characteristics and dynamic process analysis of the 2018 Mabian consequent landslide in Sichuan Province, China. *Bull. Eng. Geol. Environ.* **79**(7), 3337–3359 (2020).
9. Yue, Z. Q. & Lee, C. F. A plane slide that occurred during construction of a national expressway in Chongqing, SW China. *Q. J. Eng. Geol. Hydrog.* **35**, 309–316 (2002).
10. Li, D. L. et al. The impact of microearthquakes induced by reservoir water level rise on stability of rock slope. *Shock Vib.* **2016**, 7583108 (2016).
11. Hu, S. M. et al. Deformation law analysis of bedding slope at entrance of highway. *Tunnel. Geotech. Eng. Tech.* **36**(06), 477–482 (2022).
12. Ma, C. C. et al. Landslide mechanism of quaternary deposits with horizontal beddings under groundwater and slope excavation. *J. Eng. Geol.* **21**(06), 878–884 (2013).
13. Yan, Q. W. et al. Investigation of the strength recovery characteristics of a red-bed landslide soil by SHS and ultrasonic experiments. *Bull. Eng. Geol. Environ.* **80**(7), 5271–5278 (2021).
14. Luo, Y. B. et al. Analysis of pipe-roof in tunnel exiting portal by the foundation elastic model. *Math. Probl. Eng.* **2017**, 9387628 (2017).
15. Qiu, H. Z. et al. Deformation mechanism and collapse treatment of the rock surrounding a shallow tunnel based on on-site monitoring. *J. Mt. Sci.* **17**(12), 2897–2914 (2020).
16. Luo, Y. B. et al. Analysis of tunnel displacement accuracy with total station. *Measurement* **83**, 29–37 (2016).
17. Kaya, A. et al. Understanding the mechanism of slope failure on a nearby highway tunnel route by different slope stability analysis methods: A case from NE Turkey. *Bull. Eng. Geol. Environ.* **75**(3), 945–958 (2016).
18. Zhang, Z. G. et al. Interaction analyses between tunnel and landslide in mountain area. *J. Mt. Sci.* **14**(6), 1124–1139 (2017).
19. Lei, P. et al. Theoretical solutions for the vertical compressive stress of shallow neighbourhood loess tunnel foundation. *J. Asian Archit. Build.* **20**(4), 428–441 (2020).
20. Liu, J. H., Xie, C. J. & Rao, J. Y. Calculation model and influencing factors of surrounding rock loosening pressure for tunnel in fold zone. *Adv. Civ. Eng.* **2021**, 6678511 (2021).
21. Xu, J. S., Liu, W. C., Wang, X. R. & Du, X. L. Stability analysis of three-dimensional tunnel roofs in soil based on a modified MC criterion. *Acta Geotech.* **19**(9), 5989–6004 (2024).
22. Wang, Y. Q., Ma, C. B. & Wang, Z. F. Prediction of landslide position of loose rock mass at mountain tunnel exit. *Adv. Civ. Eng.* **2019**, 3535606 (2019).
23. Cai, Y. X. et al. Analytic study on interaction among shallow multiple circular tunnels under slope terrain. *Comput. Geotech.* **173**, 106541 (2024).
24. Zhang, Q. et al. Study on slope stability due to the influence of excavation of the high-speed rail tunnel. *Geomat. Nat. Hazards Risk* **10**(1), 1193–1208 (2019).
25. Song, D. Q. et al. Influence of tunnel excavation on the stability of a bedded rock slope: A case study on the mountainous area in Southern Anhui, China. *KSCE J. Civ. Eng.* **25**(1), 114–123 (2021).
26. Dyson, A. P. & Griffiths, D. V. An efficient strength reduction method for finite element slope stability analysis. *Comput. Geotech.* **174**, 106593 (2024).
27. Jiang, S. H. et al. Advances in reliability and risk analyses of slopes in spatially variable soils: A state-of-the-art review. *Comput. Geotech.* **141**, 104498 (2022).
28. Tschuchnigg, F., Schweiger, H. F. & Sloan, S. W. Slope stability analysis by means of finite element limit analysis and finite element strength reduction techniques Part I: Numerical studies considering non-associated plasticity. *Comput. Geotech.* **70**, 169–177 (2015).
29. Chen, J. et al. Step-path failure mechanism and stability analysis of water-bearing rock slopes based on particle flow simulation. *Theor. Appl. Fract. Mech.* **131**, 104370 (2024).
30. Tian, X. X. et al. Deformation and mechanical characteristics of tunnel-slope systems with existing anti-slide piles under the replacement structure of pile-wall. *Tunn. Undergr. Space. Technol.* **153**, 105995 (2024).
31. Tian, X. X., Song, Z. P. & Zhang, Y. W. Monitoring and reinforcement of landslide induced by tunnel excavation: A case study from Xiamaixi tunnel. *Tunn. Undergr. Space Technol.* **110**, 103796 (2021).

32. Qin, Y. W. et al. Failures in loess slope-tunnel system: An overview of trigging sources, acting mechanism and mitigation strategies. *Eng. Fail. Anal.* **158**, 107996 (2024).
33. Ding, C., Xue, K. X. & Zhou, C. H. Deformation analysis and mechanism research for stratified rock and soil slope. *Bull. Eng. Geol. Environ.* **83**(8), 300 (2024).
34. Tian, X. X., Song, Z. P., Cheng, Y. & Wang, J. B. Deformation distribution characteristics of a tunnel-slope system and its reinforcement measures. *B. Eng. Geol. Environ.* **84**(6), 271 (2025).
35. Song, D. et al. Using near-real-time monitoring of landslide deformation to interpret hydrological triggers in Jiudian Gorge Reservoir. *Indian J. Mar. Sci.* **46**(11), 20182–22190 (2017).
36. Yoshizawa, N. & Hosokawa, Y. Analysis of rotational slide using surveyed data of surface displacement in landslide area. *Landslides* **23**(4), 13–23 (2011).
37. Liu, J., Wang, J. J. & Guo, J. J. Calculation method of surrounding rock pressure of shallow buried unsymmetrical pressure tunnel in horizontal soft and hard interactive stratum. *Sci. Technol. Eng.* **22**(04), 1649–1655 (2022).

Acknowledgements

Author contributions

T.L.: Data curation, Funding acquisition, Investigation, Writing-review & editing. Y.L.: Writing-original draft, Software. J-j.S.: Methodology, Supervision, Validation. S-m.H.: Conceptualization, Formal analysis, Writing–review & editing. B.L.: Visualization, Data curation.

Declarations

Competing interests

The authors declare no competing interests.

Additional information

Correspondence and requests for materials should be addressed to Y.L.

Reprints and permissions information is available at www.nature.com/reprints.

Publisher's note Springer Nature remains neutral with regard to jurisdictional claims in published maps and institutional affiliations.